



## OPEN ACCESS

## EDITED BY

Hussein Hoteit,  
King Abdullah University of Science and  
Technology, Saudi Arabia

## REVIEWED BY

Alireza Kazemi,  
Sultan Qaboos University, Oman  
Yazhou Liu,  
China University of Petroleum, Beijing, China

## \*CORRESPONDENCE

Amirmasoud Kalantari Dahaghi,  
✉ Masoud@ku.edu

RECEIVED 12 September 2024

ACCEPTED 03 February 2025

PUBLISHED 06 March 2025

## CITATION

Emera R and Kalantari Dahaghi A (2025)  
Maximizing conventional oil recovery and  
carbon mitigation: an artificial intelligence-  
driven assessment and optimization of carbon  
dioxide enhanced oil recovery with physics-  
based dimensionless type curves.  
*Front. Energy Res.* 13:1478473.  
doi: 10.3389/fenrg.2025.1478473

## COPYRIGHT

© 2025 Emera and Kalantari Dahaghi. This is an  
open-access article distributed under the terms  
of the [Creative Commons Attribution License](#)  
(CC BY). The use, distribution or reproduction in  
other forums is permitted, provided the original  
author(s) and the copyright owner(s) are  
credited and that the original publication in this  
journal is cited, in accordance with accepted  
academic practice. No use, distribution or  
reproduction is permitted which does not  
comply with these terms.

# Maximizing conventional oil recovery and carbon mitigation: an artificial intelligence-driven assessment and optimization of carbon dioxide enhanced oil recovery with physics-based dimensionless type curves

Raghda Emera<sup>1,2</sup> and Amirmasoud Kalantari Dahaghi<sup>1,2\*</sup>

<sup>1</sup>Center for Net Carbon Zero GeoEnergy Intelligence and Sustainability (COGEIS), The University of Kansas, School of Engineering, Chemical and Petroleum Engineering Department, Lawrence, KS, United States, <sup>2</sup>The University of Kansas, School of Engineering, Chemical and Petroleum Engineering Department, Lawrence, KS, United States

**Introduction:** Carbon Dioxide Enhanced Oil Recovery (CO<sub>2</sub>-EOR) is a well-established technology that has been deployed for over 2 decades, primarily to boost oil recovery rates. Recently, however, CO<sub>2</sub>-EOR has gained attention as a potential carbon mitigation strategy, given its ability to both enhance oil recovery without requiring extensive new drilling and store CO<sub>2</sub> in subsurface formations. This dual function aligns with net-zero carbon goals, as CO<sub>2</sub> is partly trapped in the reservoir through solubility and hysteresis effects on relative permeability. The performance of CO<sub>2</sub>-EOR, in terms of both oil recovery and CO<sub>2</sub> storage potential, depends on numerous factors, including reservoir properties such as porosity, permeability, thickness, fluid composition, and operating conditions like bottom-hole pressure and injection rates. Traditional screening for CO<sub>2</sub>-EOR candidate reservoirs typically relies on experimental work, simulation studies, and field analogs, all of which require significant time and resources. However, a large dataset exists from prior CO<sub>2</sub>-EOR projects, which could enable more efficient screening.

**Methods:** To leverage this data and capitalize on recent advancements in artificial intelligence, we developed an integrated methodology to predict CO<sub>2</sub>-EOR production profiles rapidly and accurately. Using Artificial Neural Networks (ANN), we trained a proxy model (PM) with over 2,000 simulation cases based on real-world CO<sub>2</sub>-EOR projects. The model's novelty lies in its ability to generate

**Abbreviations:** AHM, Assisted History Match; AI, Artificial Intelligence; ANN, Artificial Neural Network; BBD, Box Behnken Design; BHFP, Bottom Hole Flowing Pressure; BHP, Bottom Hole Pressure; CCUS, Carbon Capture Utilization and Storage; CO<sub>2</sub>, Carbon dioxide; EOR, Enhanced Oil Recovery; GHG, Greenhouse Gas; GOC, Gas Oil Contact; HCPVI Hydrocarbon, Pore Volume Injected; LSSVM, Least Squares Support Vector Machines; MAE, Mean Absolute Error; MAPE, Mean Absolute Percentage Error; MARS, Multivariate Adaptive Regression Splines; MMP, Minimum Miscibility Pressure; MSE, Mean Squared Error; PM, Proxy Model; PVT, Pressure-Volume-Temperature; Qg, Gas Flow Rate; Qo, Oil Flow Rate; R2, Correlation of Coefficient; ReLU, Rectified Linear Unit; RMSE, Root Mean Square Error; RP, Relative Permeability; WAG, Water Alternate Gas; WOC, Water Oil Contact.

dimensionless type curves and their derivatives, which can be matched with production data to estimate average reservoir characteristics at later project stages.

**Results and Discussions:** Our results demonstrate that the proxy model achieves a high level of accuracy, with a maximum Mean Absolute Error (MAE) of 0.012 and a correlation coefficient of 0.99 between predicted and simulated results across three output variables. Additionally, a sensitivity analysis revealed the significant influence of parameters such as fluid composition, rock-fluid interaction, porosity, permeability, and initial reservoir pressure on CO<sub>2</sub>-EOR production profiles. This approach provides a rapid, cost-effective alternative to conventional methods, allowing for quicker and more informed decision-making in CO<sub>2</sub>-EOR projects.

KEYWORDS

compositional dimensionless type curves, AI-based proxy model, CO<sub>2</sub>-EOR, CCUS, CO<sub>2</sub>-EOR type curves

1 Introduction

CO<sub>2</sub> flooding, an enhanced oil recovery technique with a history spanning over 4 decades, holds promise for unlocking technically recoverable oil reserves across various global basins (GHG, 2009). Estimates suggest substantial reserves, with the Middle East alone potentially harboring up to 451 billion barrels of technically recoverable oil. In the United States, CO<sub>2</sub> flooding projects yielded around 300,000 barrels per day in 2012 (Dean et al., 2018). Notably, when sourced from industrial emissions (referred to as anthropogenic CO<sub>2</sub>), CO<sub>2</sub> used in EOR can have positive environmental implications. By capturing and injecting industrial CO<sub>2</sub> underground, it becomes sequestered within the reservoir, mitigating its atmospheric presence and reducing its contribution to the greenhouse effect. This integration has positioned CO<sub>2</sub> EOR within the framework of Carbon Capture Utilization and Storage (CCUS). In the United States, CO<sub>2</sub> EOR fields have the potential to accommodate between 55 billion to 119 billion metric tons of CO<sub>2</sub> under the “2019 View,” with projected oil production ranging from 84 billion to 181 billion barrels of stranded oil (NPC, 2019).

Various approaches to CO<sub>2</sub>-EOR are employed based on specific reservoir conditions and operational constraints. Among these

methods, miscible or immiscible flooding stands out as the most prevalent. In miscible flooding, CO<sub>2</sub> is injected at pressures sufficient to achieve full miscibility, effectively blending CO<sub>2</sub> and oil into a single liquid phase. For reservoirs characterized by extensive vertical communication—exhibited by high permeability and continuity of oil-bearing pore space in the vertical direction—a gravity-stabilized miscible flood is often favored as the optimal operational mode, as noted (Claridge, 1972).

Utilizing CO<sub>2</sub> flooding for enhanced oil recovery relies on specific criteria for identifying suitable reservoir candidates. Scholars have put forth various sets of selection criteria over the years. Initially introduced by Taber et al. (1997) (Taber et al., 1997) and subsequently refined by (Aladasani and Bai, 2010), these criteria have been further elucidated by (Yin, 2015) with a focus on US fields. A comprehensive overview of these selection criteria, as outlined by the aforementioned researchers, is presented in Table 1.

In recent years, numerous researchers have explored the application of diverse machine learning algorithms in the design of enhanced oil recovery (EOR) projects, with a particular emphasis on CO<sub>2</sub> flooding strategies. For instance, a deep learning classifier has been employed to forecast the optimal EOR approach by considering multiple factors, including lithology, reservoir

TABLE 1 CO<sub>2</sub> selection criteria range (Yin, 2015).

	Taber et al. (1997)	Aladasani and Bai (2010)	Gao and Pan (2010)	Yin (2015)	
				Sandstone	Carbonate
Porosity (%)		3–37	>12	7–295	4–23.7
Permeability (mD)			>10	>10	>2
Gravity (°API)	>22	28–45	>27	>27	>28
Viscosity (cp)	<10	0–35	<10	<3	<6
Temperature (°F)		82–250		83–260	86–232
Depth (ft)		1,500–13,365	>2,500	1,150–11,950	3,000–11,100
Oil Saturation (%)	>20	15–89		>20	
Water Flooding Recovery Factor			20%–50% OOIP		
Net Thickness (ft)				15–268 (75–137)	

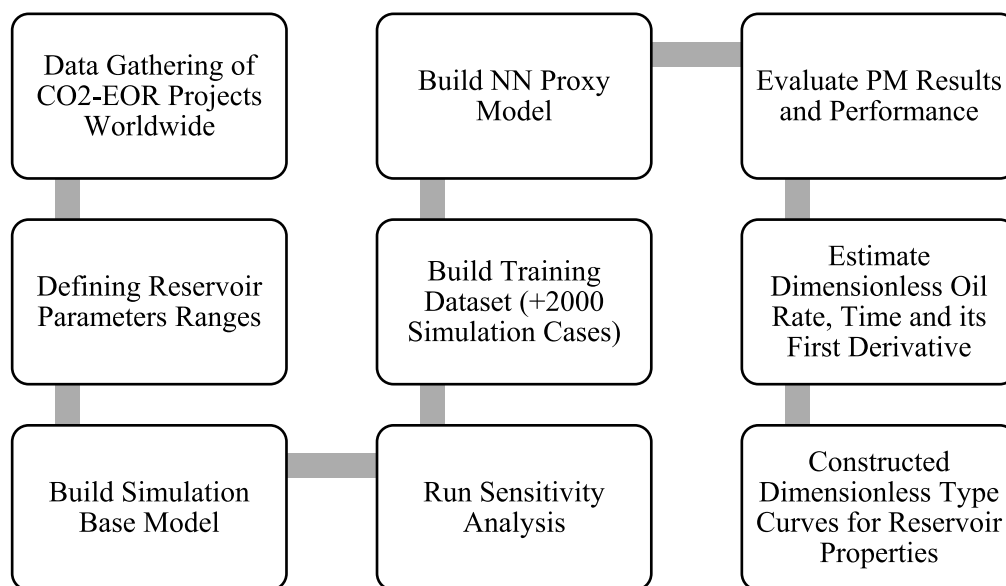


FIGURE 1  
Phase envelope of PVT templates.

characteristics such as depth, porosity, and permeability, as well as reservoir fluid properties like oil gravity and viscosity. Remarkably, this classifier achieved an impressive accuracy level of up to 95% (Kumar Pandey et al., 2023). Additionally, artificial neural network (ANN) algorithms offer a means to investigate the behavior of pure CO<sub>2</sub> foam in porous media and its rheological properties, offering an alternative to labor-intensive laboratory experiments in the context of CO<sub>2</sub> EOR and sequestration endeavors (Iskandarov et al., 2022).

Furthermore, machine learning techniques enable the preliminary evaluation of CO<sub>2</sub> storage in residual oil zone reservoirs under various scenarios, such as continuous CO<sub>2</sub> injection or WAG (water alternating gas), aiding in the determination of CO<sub>2</sub> storage capacity. Notably, the Multivariate Adaptive Regression Splines (MARS) technique has demonstrated superior accuracy in this context (Chen and Pawar, 2019).

Proxy models serve as efficient tools that swiftly provide insights typically derived from extensive simulation studies. These models are based on predefined parameter equations and leverage hybrid machine learning algorithms such as least squares support vector machines (LSSVM) and box-Behnken design (BBD) to generate predictions, notably exhibiting satisfactory results in forecasting oil recovery factors in CO<sub>2</sub> injection scenarios (Ahmadi et al., 2018).

Carbon dioxide is recognized as one of the greenhouse gas emissions (GHG). Reports indicate that between 2006 and 2015, approximately 38 giga metric tons per year of CO<sub>2</sub> were discharged into the atmosphere from anthropogenic sources, encompassing activities such as fossil fuel emissions and land-use changes. Despite the capacity of ocean and terrestrial plants to act as sinks for CO<sub>2</sub>, thereby reducing its atmospheric concentration, the rate of emissions surpasses the sink's capacity, resulting in an annual accumulation of CO<sub>2</sub> in the atmosphere at a rate of 2 parts per million (ppm) (Le Quéré et al., 2016). Globally, nations have committed to attaining carbon emission neutrality, with 90% of

them targeting 2050 as the deadline for this objective, while others aim for 2060. Carbon Capture, Utilization, and Storage (CCUS) emerges as a climate change mitigation strategy, involving the capture of emitted CO<sub>2</sub> from stationary sources and subsequent distribution for either utilization or storage purposes (Tapia et al., 2018). Geological storage of CO<sub>2</sub> in subsurface formations represents a viable pathway towards achieving net zero emissions goals. Such storage can take various forms, including injection into saline aquifers, depleted oil reservoirs, or CO<sub>2</sub>-EOR projects. Given that only a fraction (50%–67%) of injected CO<sub>2</sub> in EOR projects is recoverable at the surface alongside produced oil, the remainder is sequestered in the subsurface (Orr, 2018). CO<sub>2</sub>-EOR projects exhibit 37% lower emissions per barrel compared to other production methods (Novak Mavar et al., 2021). Unlike other underground CO<sub>2</sub> storage projects, CO<sub>2</sub> EOR projects are economically advantageous as they enhance oil production, which can be monetized for a net profit, while other injection projects rely solely on government-provided tax reduction incentives (Novak Mavar et al., 2021). An essential performance metric for evaluating the success of CO<sub>2</sub> storage in CO<sub>2</sub> EOR is the estimation of the CO<sub>2</sub> Retention Factor, defined as:

$$\text{CO}_2 \text{ Retention \%} = \frac{\text{CO}_2 \text{ Remaining at Subsurface}}{\text{Cumulative CO}_2 \text{ Injected}} \times 100 \quad (1)$$

In CO<sub>2</sub>-EOR projects across the United States, retention factors vary between 28% and 98.7% for both continuous and WAG injection methods, contingent upon reservoir parameters, lithology, and the volume of hydrocarbon pore volume injected (HCPVI). In miscible CO<sub>2</sub> flooding endeavors, an increase in the injected CO<sub>2</sub> HCPVI correlates with a reduction in the retention factor (Olea, 2015).

In this research, an initial compositional simulation model served as the foundation. Eight synthetic fluid composition templates and nine synthetic relative permeability templates were

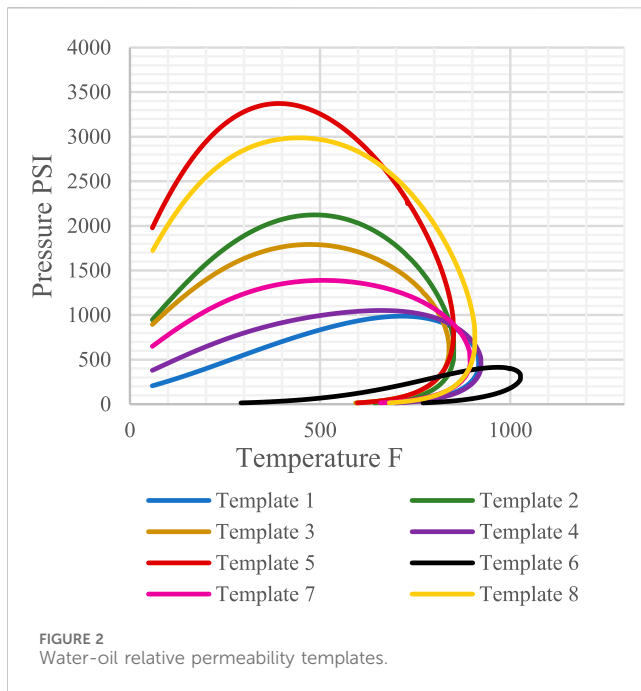


FIGURE 2  
Water-oil relative permeability templates.

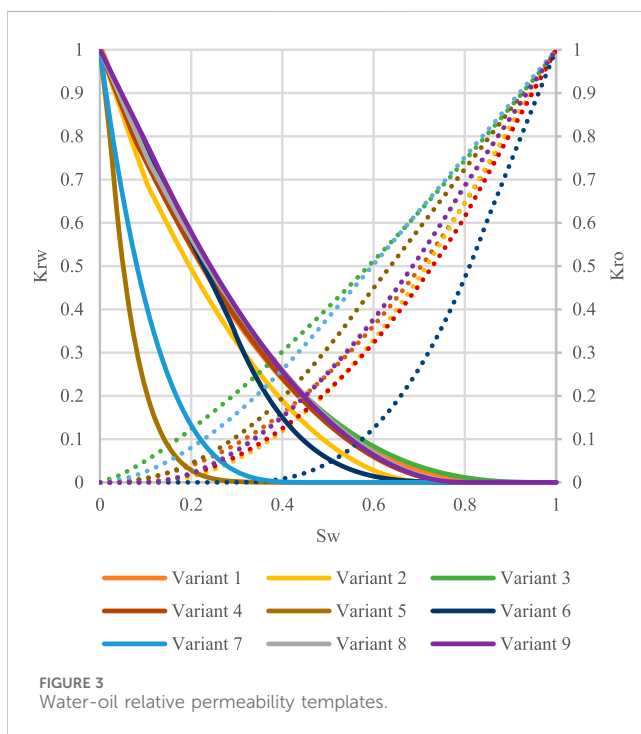


FIGURE 3  
Water-oil relative permeability templates.

developed, encompassing a wide spectrum of data found in the literature [Figures 1, 2](#). Additionally, ranges for reservoir properties such as porosity, permeability, and initial reservoir pressure were defined based on published CO<sub>2</sub>-EOR projects. Then using Latin hypercube sampling generated more than 2000 simulation cases. The simulation results dataset is used to build the proxy model which is then used to predict the results and generate dimensionless type curves. The workflow of the research is shown in [Figure 3](#).

## 2 Numerical reservoir simulation

The investigation utilized the tNavigator Compositional module, a commercial software package. The fundamental equation dictating flow within porous media is the Mass Conservation equation for each component, as outlined by ([Chen et al., 2006](#)) in [Equation 2](#):

$$\frac{\partial}{\partial t} (\phi c_i \rho_i) = -\nabla \cdot \left( \sum_{\alpha=1}^{N_p} \rho_i [c_{i\alpha} u_{\alpha} - D_{i\alpha} \nabla c_{i\alpha}] \right) + q_i \quad (2)$$

$$i = 1, 2, \dots, N_c$$

where:

$c_i$  are the overall concentration phases,  $N_p$  is the number of phases,  $\rho_i$  mass density,  $q_i$  is source/sink term,  $c_{i\alpha}$  and  $D_{i\alpha}$  are concentration and diffusion-dispersion tensor of component  $i$  in phase  $\alpha$ .

The base model comprises a box configuration encompassing 64,000 cells, all possessing identical vertical and horizontal permeability within the reservoir. Porosity remains constant at a single value as specified in [Table 2](#). This model features two wells: one functioning as a producer and the other as an injector. The controlling mode for both is the Bottom hole Pressure. Injection operations lasted for 30 years commenced on day 1 to uphold pressure levels, with the bottom hole flowing pressure (BHFP) limit set 1,470 psi to be higher than both the minimum miscibility pressure (MMP) and the bubble point pressure, ensuring single-phase flow within the reservoir and the bottom hole injection pressure set to be 6,000 psi to ensure that it does not exceed fracture pressure. The maximum production rate was set to be 5000 STB/D and maximum injection rate is 10,000 MSCF/D. Initial conditions were established within the oil production zone, devoid of free water or gas, situated above the oil-water contact, and below the gas-oil contact [Table 2](#). Using template one of the defined fluid composition and relative permeability templates.

## 3 Dimensionless curves

Drawing upon the pioneering work of ([Arps, 1945](#)) in decline curve analysis, the normalization of rates based on post-flow rates has been applied in multiphase flow analysis as introduced by ([Fetkovich and Vienot, 1984](#)), alongside other type-curves for various assessments ([Doublet and Blasingame, 1995](#)). Blasingame further delved into decline curve analysis in the context of secondary recovery scenarios involving water influx and waterflood cases. In the present study, we computed dimensionless oil rate using [Equation 3](#) and time using [Equation 4](#), along with their first derivative, serving as a diagnostic tool for reservoir properties. The definition of dimensionless numbers aligns with that employed by ([Fetkovich, 1973](#)).

### 3.1 Dimensionless rate

$$q_D = \frac{141.2 \times q \times \mu \times \beta}{K \times h \times (P_i - BHFP)} \times \frac{L}{W} \quad (3)$$

TABLE 2 Base model description.

Property	Value
No. of blocks in the X direction	80
No. of blocks in the Y direction	80
No. of blocks in the Z direction	10
Step length in X direction dx (ft)	50
Step length in Y direction dy (ft)	50
Step length in Z direction dz (ft)	10
Porosity (Fraction)	0.12
Horizontal Permeability $K_x = K_y$ (mD)	16
Vertical Permeability $K_z$ (mD)	$0.1 * K_x$
Datum depth (ft)	5,300
Datum Initial Pressure (Psi)	3,000
Water Oil Contact (WOC) (ft)	5,500
Gas Oil Contact GOC (ft)	0
Rock Compressibility (1/psi)	$3.4 \text{ e-}06$

### 3.2 Dimensionless time

$$t_D = \frac{0.00634 \times K \times t}{\phi \times \mu \times C_t \times r_w^2} \quad (4)$$

Where  $q$  is the production oil flow rate in STB/day,  $\mu$  is the oil viscosity in cp,  $\beta$  is the oil formation volume factor in bbl/STB,  $K$  is the reservoir permeability,  $h$  is the reservoir thickness,  $P_i$  is the reservoir initial pressure in Psi,  $BHFP$  is the bottom hole flowing pressure in Psi,  $\phi$  is the reservoir porosity,  $C_t$  is the total compressibility in 1/psi,  $r_w$  is the wellbore radius.

Calculating the first derivative of the dimensionless oil flow rate using the Bourdet method as shown in Equation 5 (Bourdet et al., 1989):

$$dQ_d = \frac{\left( \frac{\Delta Q d_1}{\Delta t_1} \Delta t_2 + \frac{\Delta Q d_2}{\Delta t_2} \Delta t_1 \right)}{\Delta t_1 + \Delta t_2} \quad (5)$$

Where,  $\Delta Q d_1$  is the change of dimensionless oil rate,  $\Delta t_1$  is the change of dimensionless time, 1 and 2 are at two consecutive points.

We noted several recurring patterns within the generated dimensionless curves:

1. In the later stages of production, three distinct regions emerge, as illustrated in Figure 4:
  - Pre-decline: Initial stable production occurs at the maximum allowable rate; preceding water or gas breakthrough, the slope is nearly flat.
  - Decline: The onset of oil rate decline is marked by a trough in the first derivative; alterations in reservoir and operational parameters affect the width, depth, location of the trough, and steepness of the slope on the curves.
  - Post-Decline: Once the production rate nears its minimum value, minimal changes occur, resulting in the first derivative slope being nearly flat.

2. The alteration in slope within the trough area is influenced by changes in oil rate, gas rate, and water rate profiles. Typically, following breakthrough, the gas rate continues to rise, whereas the water rate increases initially before declining thereafter. This transition often yields a secondary shallower trough as depicted in Figures 5, 6.
3. The derived slopes pertain to the late-time production trough. We specifically identified four slopes to capture variations, though additional definitions are possible. The extent of the trough vertically is governed by the lowest point in the curvature, while its width encompasses both primary and secondary troughs, estimated as the entire region between two zero slopes, as depicted in Figure 4.

## 4 Parameters' sensitivity

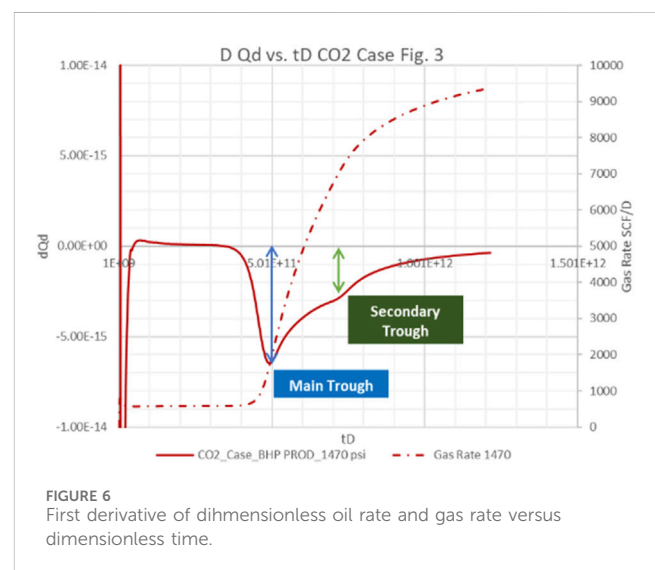
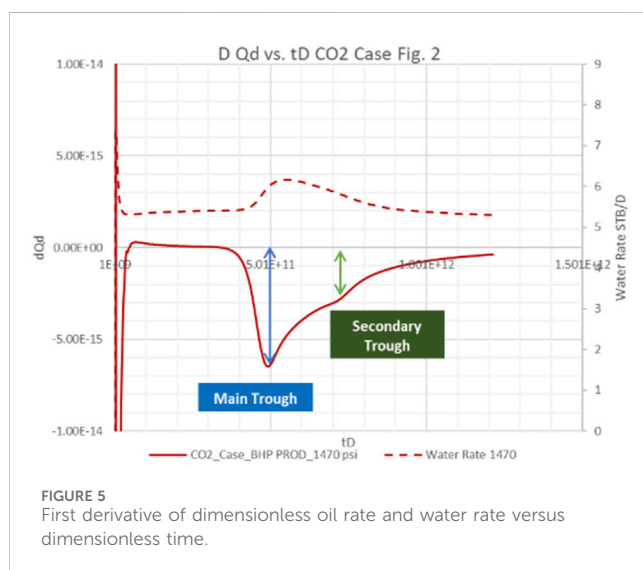
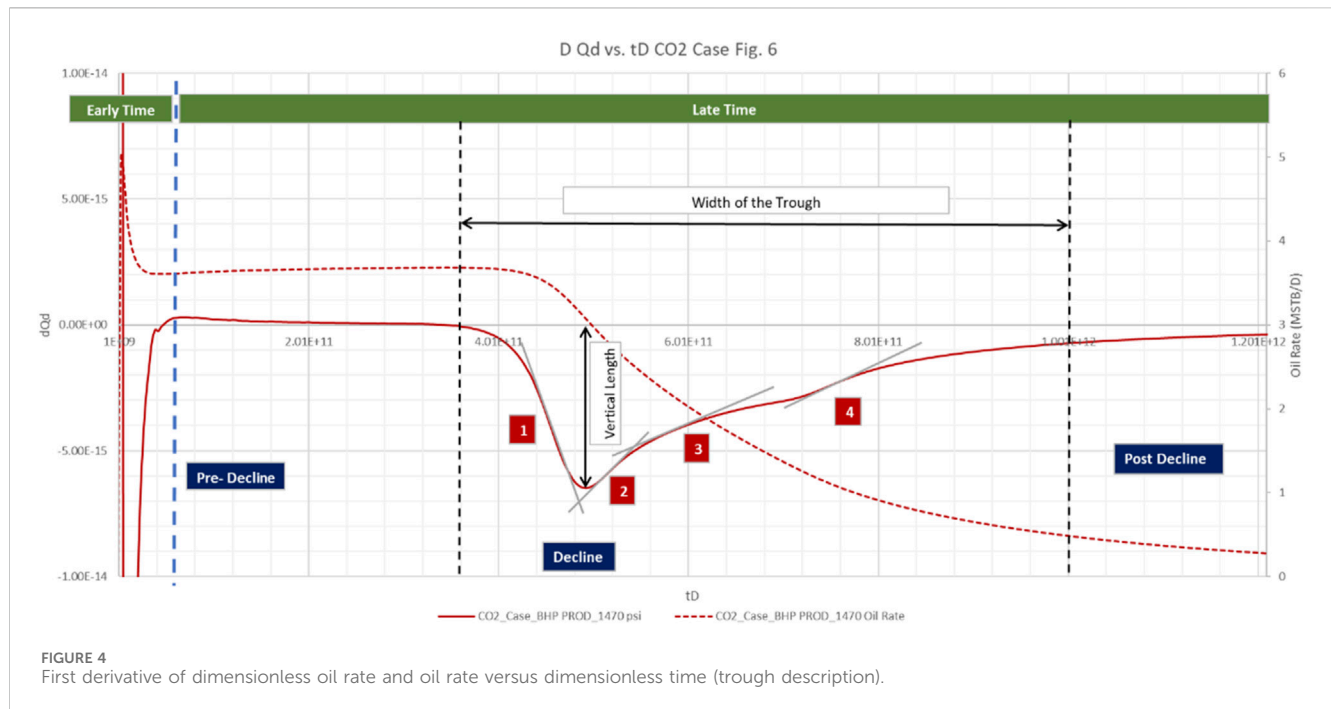
In this segment, a sensitivity analysis was performed on the base model, where one parameter was altered at a time while keeping all other reservoir variables constant. This aimed to assess their influence on production. We examined the repercussions of modifying reservoir properties in specific range, including fluid composition on 8 templates, rock-fluid interaction on 9 templates, porosity in the range of 0.05 and 0.385, permeability in the range of 2 and 980 mD, and initial pressure in the range of 1,500 psi and 5,000 psi, alongside operational factors like the bottomhole flowing pressure of the producer well in the range of 1,470 psi and 4,764 psi. Diagnostic plots employed for comparison encompassed dimensionless type curves, oil recovery factor, and  $\text{CO}_2$  retention factor plotted against the hydrocarbon pore volume injected, as well as oil, gas, and  $\text{CO}_2$  molar production rates.

### 4.1 Fluid composition sensitivity

The recovery efficiency of  $\text{CO}_2$  flooding EOR is influenced by the composition of the oil. Optimal displacement efficiency is attained at a minimal miscibility pressure, which correlates inversely with the weight percentage of hydrocarbons ranging from C5 to C30 (Holm and Josendal, 1982). The presence of light components such as C2 to C4 in reservoir oil does not significantly affect the recovery process, as these gases tend to channel and bypass the miscible bank. However, the inclusion of methane (C1) in reservoir oil diminishes the overall recovery efficiency (Holm and Josendal, 1974).

The suggested scope for employing  $\text{CO}_2$  miscible flooding in oil reservoirs is for those with an API gravity exceeding 30. As the gravity of reservoir oil rises, its viscosity diminishes, leading to a more advantageous mobility ratio and improved sweeping efficiency. Additionally, with increasing oil gravity, there is a greater presence of intermediate components (C5-C20) which undergo condensation or vaporization processes necessary for achieving miscibility (Klins, 1984). Factors such as reservoir temperature, critical properties, and bubble point pressure influence the minimum miscibility pressure attained (Holm and Josendal, 1982).





Data extracted from literature on prominent CO<sub>2</sub> flooding projects revealed a variation in oil density ranging from 25 to 45 API, with prevalent values, concentrated within the 35 to 40 API range. Reservoir temperatures spanned from a minimum of 83°F to a maximum of 267°F, while bubble point pressures exhibited a range of 300–2200 PSI. Minimum Miscibility Pressure values were observed to fluctuate between 900 and 4500 PSI, with the majority clustering within the 1,100 to 2,500 PSI range.

Subsequently, after compiling fluid composition data from 14 significant CO<sub>2</sub> flooding sites, eight templates were generated to represent the characteristics found in the literature. These templates were then utilized in constructing simulation scenarios, as depicted in Table 1 in supplemental material. The templates cover

a range of oil density from 21 to 109 API, bubble point pressures spanning 103 to 2625 PSI, and MMP ranging from 1,090 to 3,460 PSI.

The employed PVT templates vary in composition and reservoir temperatures, resulting in varied behaviors regarding oil recovery and storage capacity were shown in Figure 7. Under consistent conditions, we observed that Template\_7 yielded the highest initial oil rate, with a corresponding decrease in the initial oil rate anticipated as the oil's API gravity diminishes.

Template\_8 and Template\_3 exhibited deviations from this pattern owing to additional characteristics influencing their performance. Despite Template\_8 having the highest API gravity, which typically implies the highest recovery, its oil composition features a notably high percentage of C<sub>1</sub>, elevating the bubble point

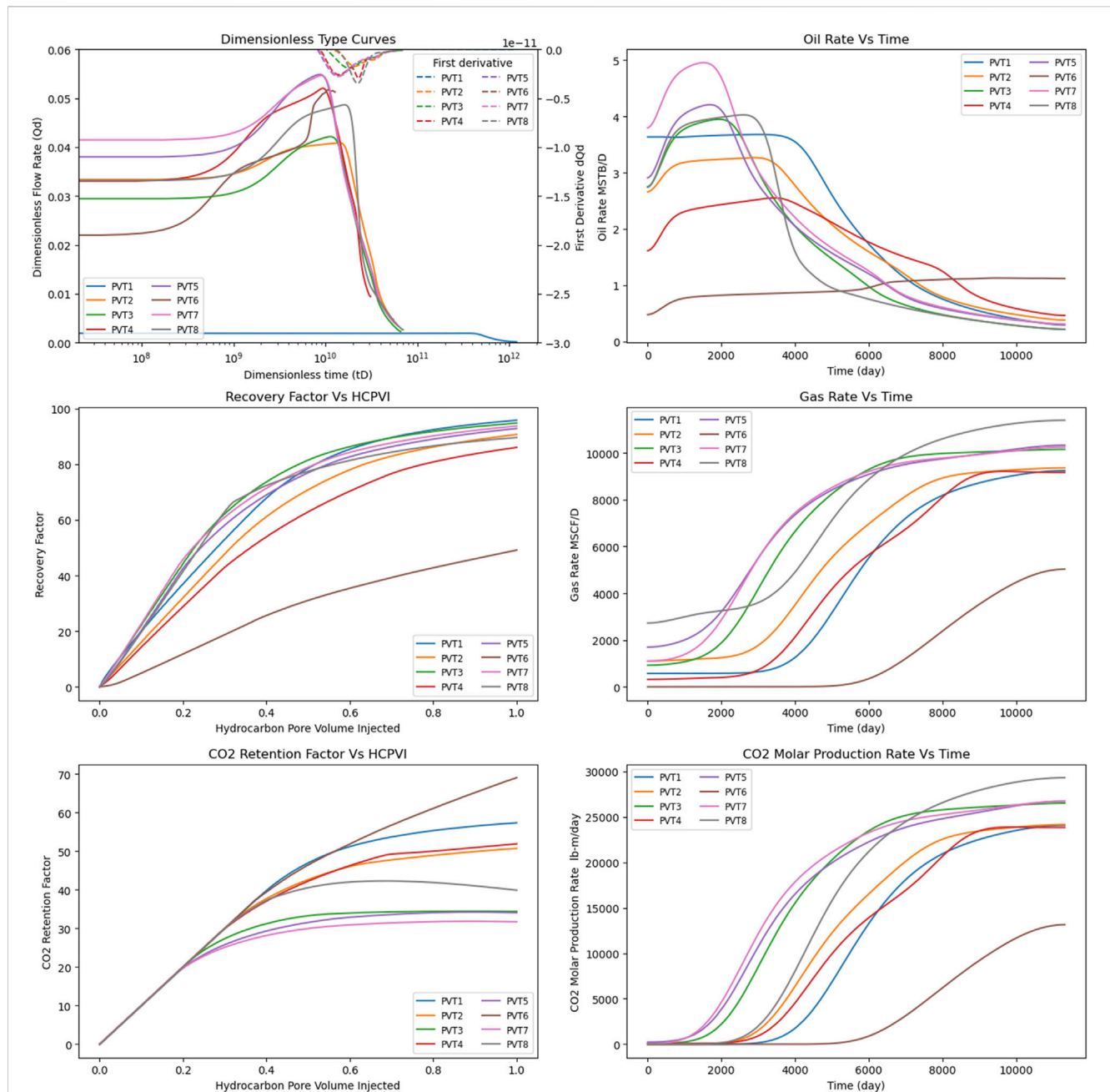


FIGURE 7  
PVT Templates Sensitivity Analysis, starting from the top left is Dimensionless Rate and its first Derivative vs dimensionless time, Recovery Factor vs standard HCPVI, CO<sub>2</sub> Retention Factor Vs HCPVI, Oil Rate, Gas Rate, and CO<sub>2</sub> Production Moles Vs Time.

pressure to 2,625 psi. Given that the set bottom hole flowing pressure is approximately 1,470 psi, lower than the bubble point, some oil molecules may have vaporized into gas, thereby augmenting the gas-oil ratio at the expense of oil rate production.

Template\_3, despite having a lower API value compared to Template\_2 and Template\_1, exhibited a higher initial oil rate. This outcome may be attributed to its higher percentage of intermediate components (C5-C20), which are conducive to the multiple evaporation and condensation processes essential for miscible recovery. In terms of recovery factor, while Template\_1 did not attain the highest initial oil rate, its production decline occurred later, enabling the accumulation of a greater

cumulative oil total and consequently, the highest recovery factor. Conversely, Template\_6, characterized by the highest C21+ component, yielded the lowest recovery factors. CO<sub>2</sub> retention factors varied among templates; Template\_6 achieved the highest CO<sub>2</sub> retention factor, with the template featuring the lowest C1 content exhibiting the lowest gas production. Template\_7 recorded the lowest CO<sub>2</sub> retention.

Among the dimensionless oil rates, Template\_7 exhibits the highest value, reflecting its superior oil rate. Meanwhile, Template\_8 displays the deepest trough in the first derivative of the oil rate.

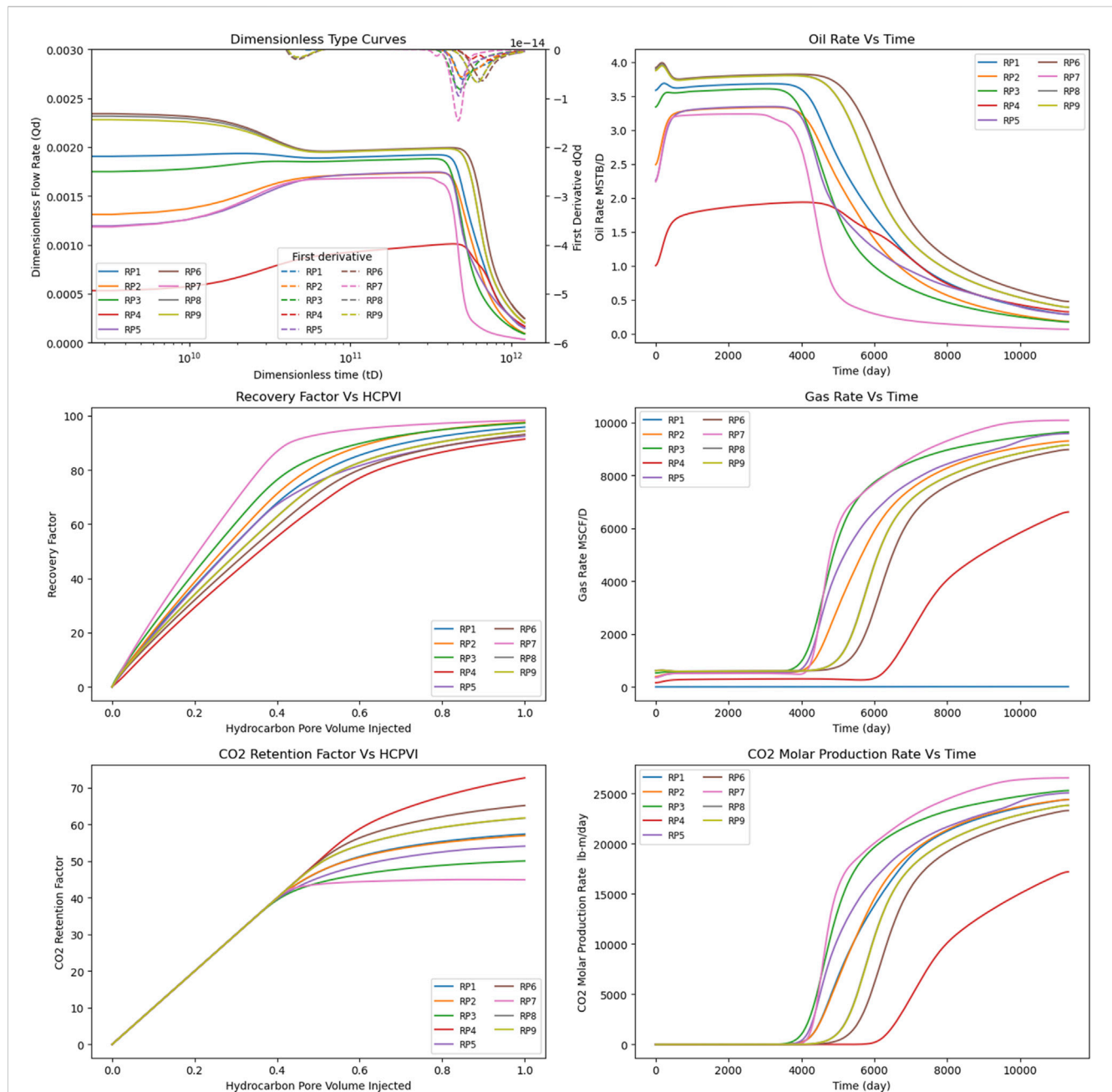


FIGURE 8  
RP Templates Sensitivity Analysis, starting from the top left is Dimensionless Rate and its first Derivative vs dimensionless time, Recovery Factor vs standard HCPVI, CO<sub>2</sub> Retention Factor Vs HCPVI, Oil Rate, Gas Rate, and CO<sub>2</sub> Production Moles.

## 4.2 Relative permeability sensitivity

Given that fluid flow within porous media involves multiple phases—oil, gas, and water—alongside CO<sub>2</sub> displacement of oil and water in CO<sub>2</sub> flooding scenarios, either immiscible or miscible, where CO<sub>2</sub> and oil blend into a single non-wetting phase, the saturation of each phase fluctuates during production initiation. Thus, relative permeability curves are indispensable for elucidating the effective permeability of each phase. Various factors influence the behavior of relative permeability curves, including rock composition, wettability, pore size distribution, interfacial tension, and phase viscosity. Relative permeability curves were

compiled from literature sources of common fields and categorized into templates based on rock type, viscosity ratio (oil to water), and interfacial tension. Twenty-one samples of relative permeability curves from reservoir fields were utilized, undergoing smoothing via Corey correlation. The parameters of the Corey Correlation of the 9 templates are presented in the [Supplementary Table S2](#).

Under constant parameters, modifications to the utilized relative permeability curve templates lead to alterations in production behavior as shown in [Figure 8](#). Template<sub>6</sub> demonstrates the highest oil production rate and dimensionless rate among all templates. Conversely, Template<sub>4</sub> exhibits the lowest production rates,



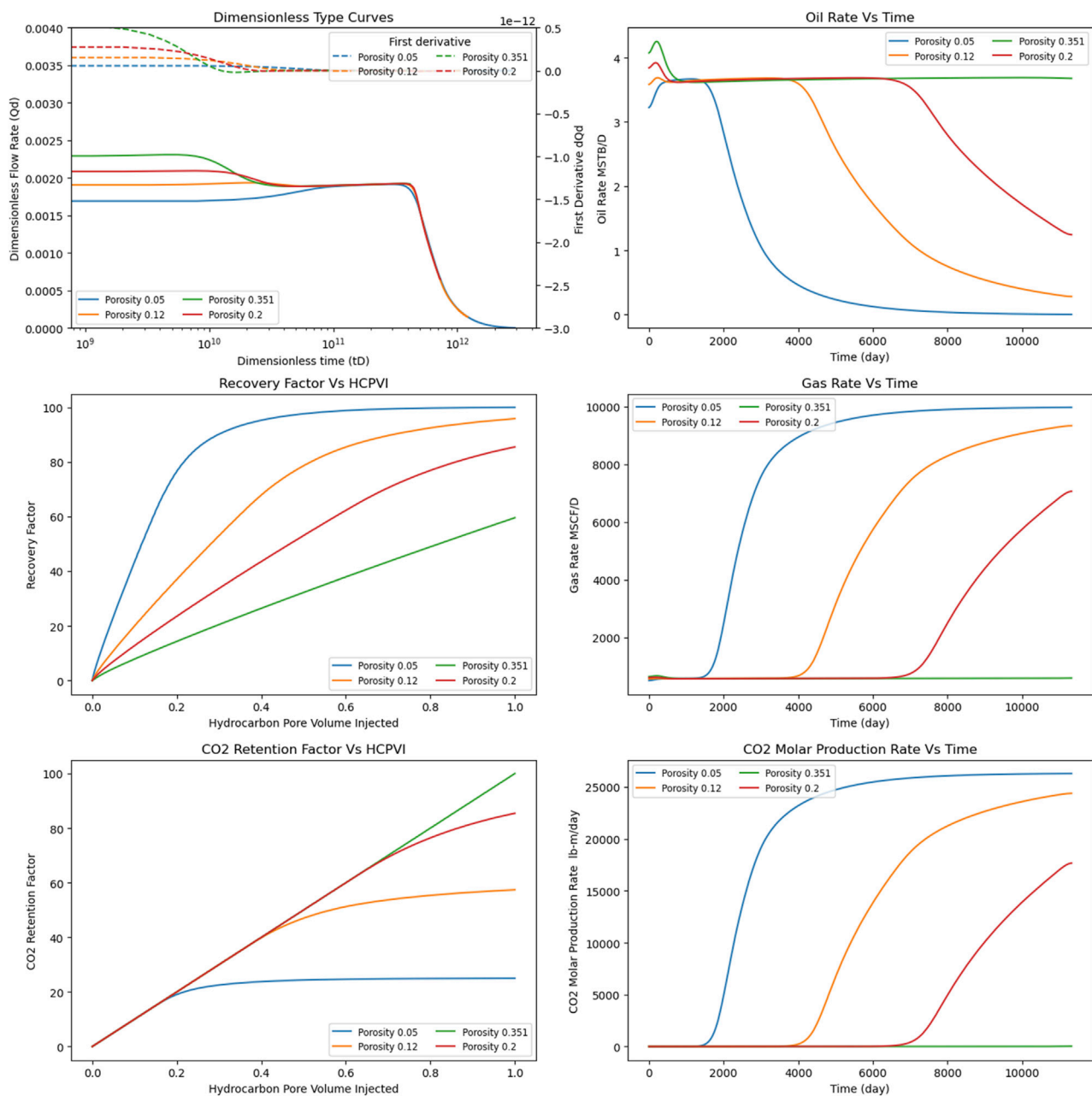


**FIGURE 9**  
Porosity Sensitivity Analysis, starting from the top left is Dimensionless Rate and its first Derivative vs dimensionless time, Recovery Factor vs standard HCPVI, CO<sub>2</sub> Retention Factor Vs HCPVI, Oil Rate, Gas Rate, and CO<sub>2</sub> Production Moles Vs Time.

attributed to its highest capillary pressure among the templates, a characteristic reflected in its elevated CO<sub>2</sub> retention factor. In contrast, Template\_7, characterized by the lowest capillary pressure, facilitates earlier gas and CO<sub>2</sub> breakthroughs, resulting in a lower CO<sub>2</sub> retention factor. The influence of capillary pressure is further evidenced in the derivative of the dimensionless oil rate, with Template\_7 showing the deepest trough, indicating a rapid rate of decline, while Template\_4 exhibits the shallowest trough, indicative of its high capillary pressure.

### 4.3 Porosity sensitivity

As porosity increases, the dimensionless oil rate also increases, albeit with a quicker initial decline, resulting in a deeper trough. However, production subsequently, stabilizes for an extended duration, potentially without experiencing a secondary trough observed in other cases. Conversely, gas and CO<sub>2</sub> molar production rates rise with decreasing porosity, leading to a decrease in the CO<sub>2</sub> retention factor. The results for the sensitivity of porosity are shown in Figure 9.

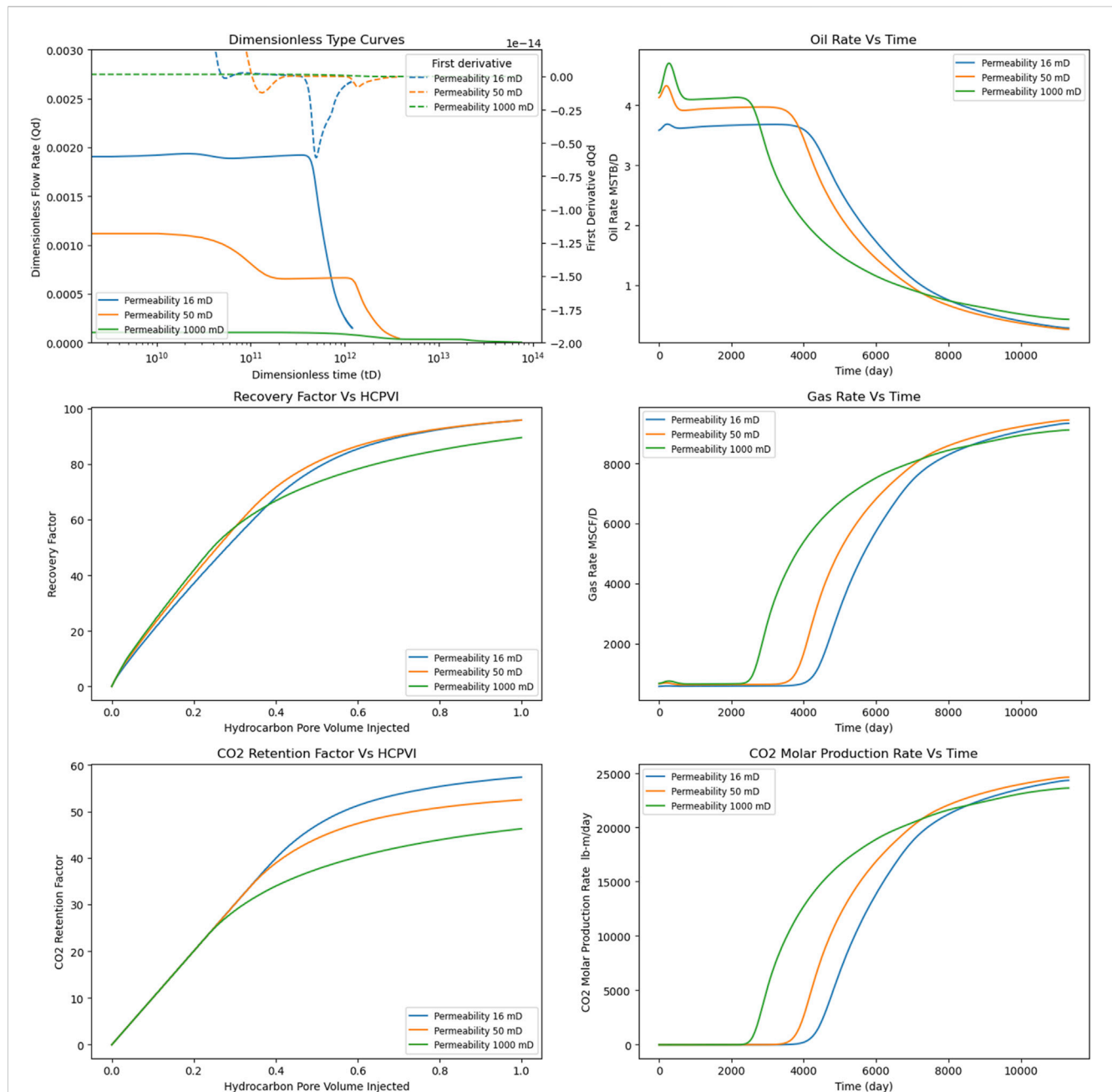


FIGURE 10 Permeability Sensitivity Analysis, starting from the top left is Dimensionless Rate and its first Derivative vs dimensionless time, Recovery Factor vs standard HCPVI, CO<sub>2</sub> Retention Factor Vs HCPVI, Oil Rate, Gas Rate, and CO<sub>2</sub> Production Moles Vs Time.

#### 4.4 Permeability sensitivity

As permeability decreases, the oil rate increases, albeit with a swifter decline due to the ease of gas breakthrough, consequently diminishing the ultimate oil recovery factor. The dimensionless oil rate demonstrates an increase, accompanied by an earlier onset of the decline stage and a shallower trough in the first derivative. The optimal oil recovery factor is observed at moderate permeability values around 50 mD. While high permeability values enhance oil flow, they accelerate water and gas breakthroughs, thereby reducing recovery. Conversely, lower permeability yields better values for CO<sub>2</sub> retention, attributed to

enhanced CO<sub>2</sub> storage resulting from solubility. The results for the sensitivity of permeability are shown in Figure 10.

#### 4.5 Initial reservoir pressure sensitivity

The initial pressure must exceed the BHFP to ensure adequate drawdown. A higher initial pressure results in a prolonged period of stabilized rate initially, yet thereafter, its influence on oil recovery, gas, or CO<sub>2</sub> production diminishes. However, distinctions can be noticed in the dimensionless rate and its first derivative with varying initial pressures.

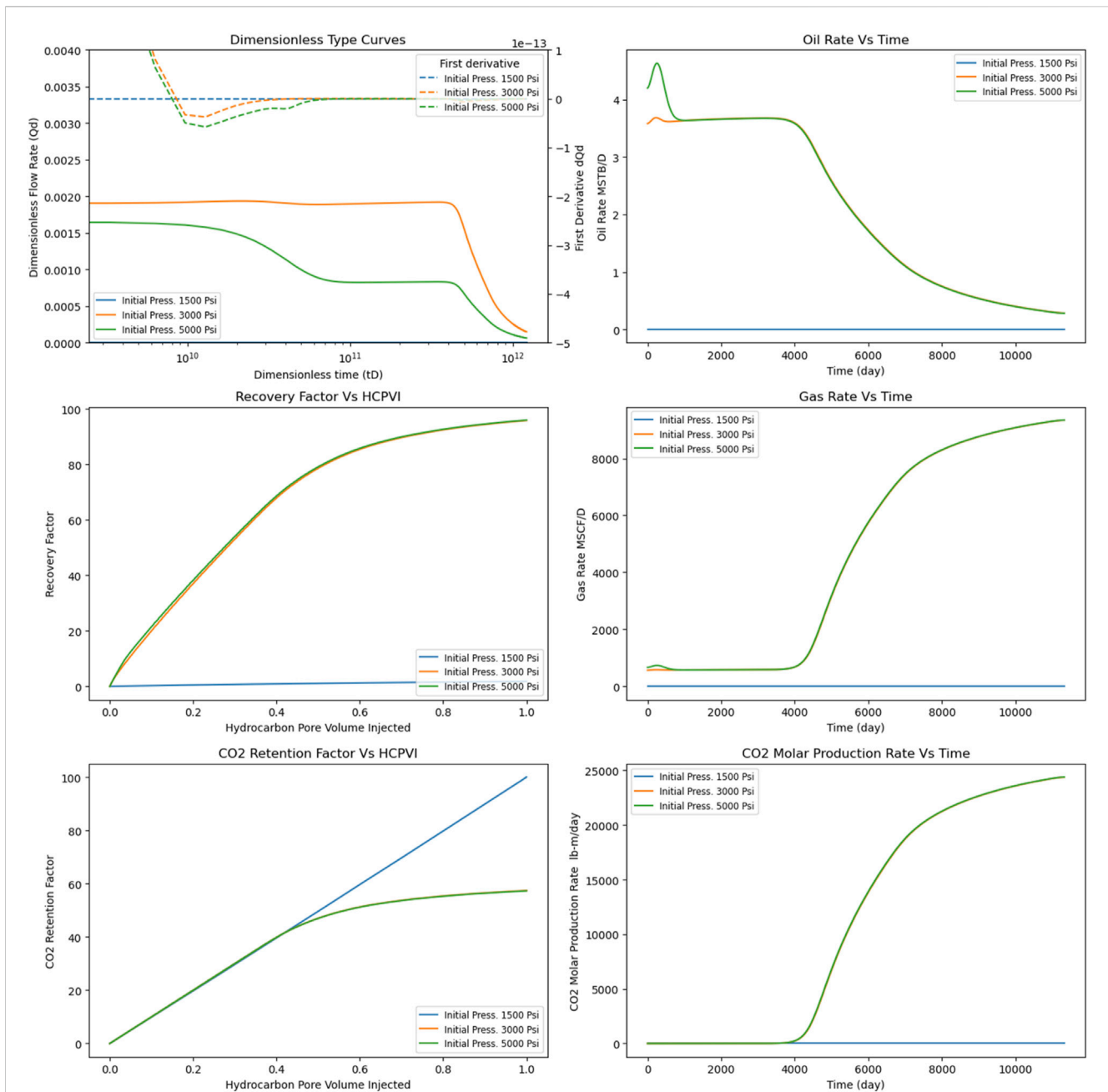


FIGURE 11 Initial Reservoir Pressure Sensitivity Analysis, starting from the top left is Dimensionless Rate and its first Derivative vs dimensionless time, Recovery Factor vs standard HCPVI, CO<sub>2</sub> Retention Factor Vs HCPVI, Oil Rate, Gas Rate, and CO<sub>2</sub> Production M.

As the initial pressure rises, the dimensionless rate decreases, and its first derivative exhibits a deeper trough. The results for the sensitivity of initial reservoir pressure are shown in Figure 11.

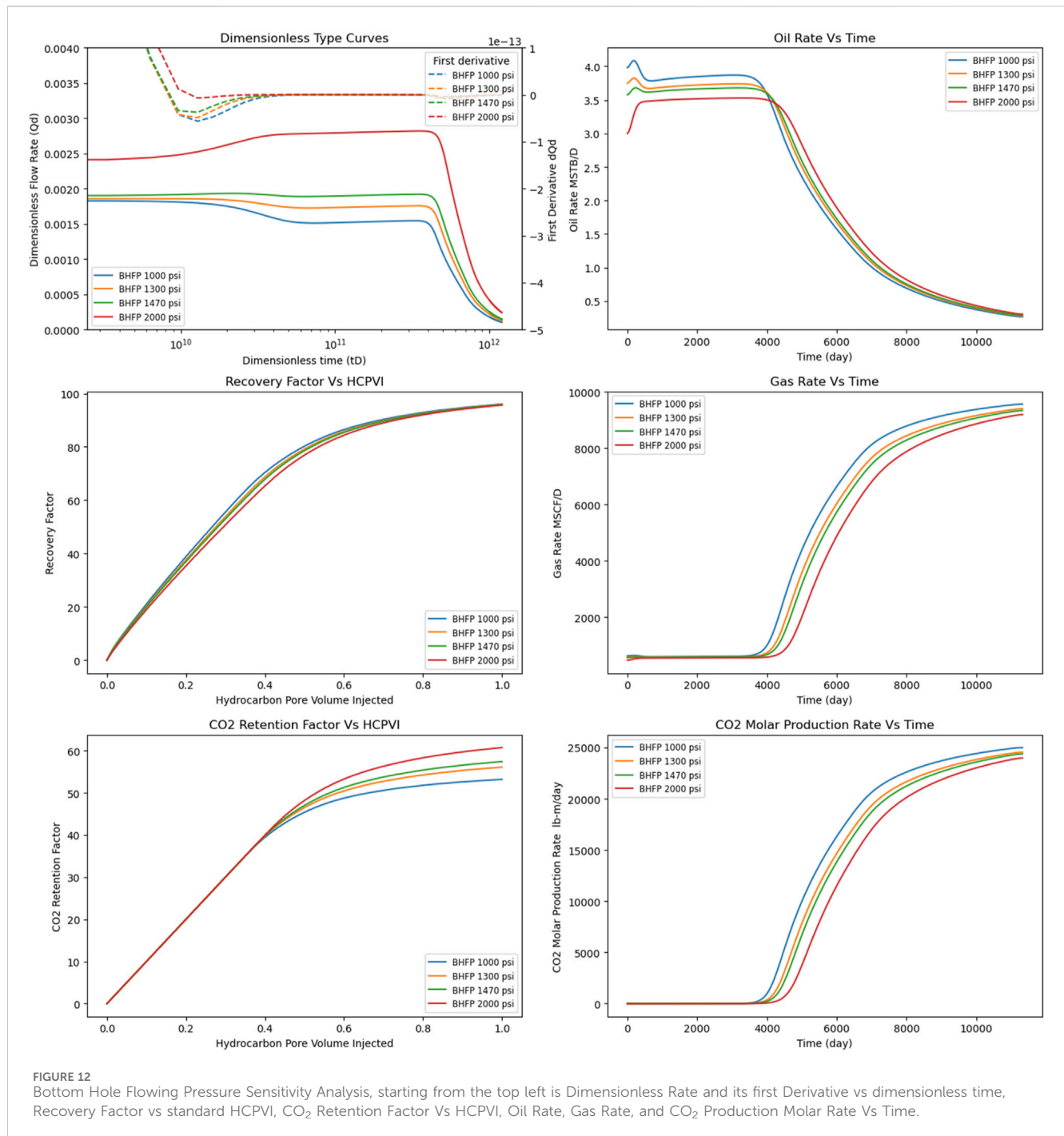
gas and CO<sub>2</sub> molar production decreases, leading to an improvement in the CO<sub>2</sub> retention factor. The results for the sensitivity of bottom hole flowing pressure are shown in Figure 12.

## 4.6 Bottom hole flowing pressure sensitivity

When the Bottom Hole Flowing Pressure (BHFP) remains higher than the Minimum Miscibility Pressure (MMP), an increase in the BHFP of the producer well corresponds to an increase in the dimensionless oil rate, along with a shallower trough in its derivative. Although the oil rate decreases, it takes slightly longer to enter the decline phase. Meanwhile,

## 5 Dataset development

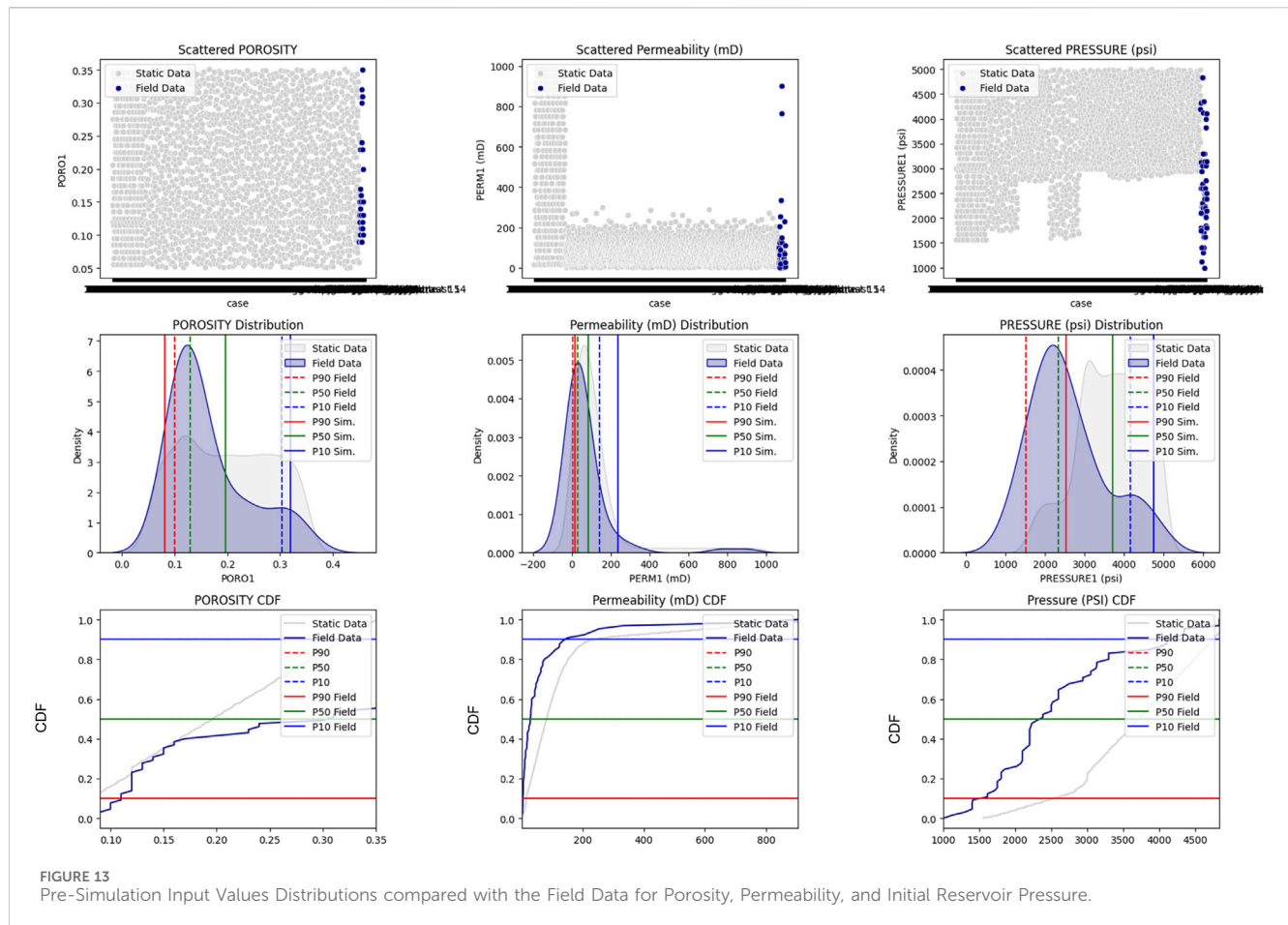
Our aim in this stage is to acquire a dataset that accurately represents the reservoir field data of the CO<sub>2</sub> EOR application, which will serve as the training data for the machine learning model. To achieve this, we employed the compositional box model utilized in the sensitivity analysis as the foundational



model for simulation work, utilizing tNavigator reservoir simulation software modules to generate the requisite data. To encompass a wide range of conditions, we conducted experiments in two phases. The variable parameters were selected based on the common selection criteria for CO<sub>2</sub>-EOR projects found in the literature, as shown in Table 1, with some modifications to suit our approach. Instead of defining reservoir fluid properties such as viscosity, API, and MMP directly, we used predefined PVT templates. Similarly, instead of relying on saturation and different rock types, we employed various relative permeability templates to represent these properties.

Initially, we developed base models with varying reservoir fluid properties and relative permeability, resulting in the creation of 8 reservoir fluid composition templates and 9 relative permeability templates. These templates were constructed based on field data obtained from the literature. By combining each PVT template with each relative permeability template, we generated a total of 72 base model cases. Throughout these base cases, porosity, permeability, and initial pressure remained constant.

In the second phase, we varied the porosity, permeability, and initial pressure for each of the 72 base models. We employed the Assisted History Matching (AHM) module to conduct a Latin



hypercube experiment for each case, running 30 model iterations per case. This process yielded a total of 2,160 models after filtering out cases with errors.

The Latin Hyper Cube algorithm operates by generating model variations according to the user-specified number of variants, denoted as  $N$ , and the number of variables, denoted as  $M$ . It partitions the search space into  $N$  hyperplanes, with each hyperplane containing precisely one variant. This method aids in covering a wide range of possibilities within the search space (McKay, 1992).

Each of the 72 cases served as a base scenario, from which 30 sensitivity cases were derived by adjusting the porosity, permeability, and initial reservoir pressure. To ensure comprehensive coverage, we employed the Latin hypercube experiment. The parameter ranges were determined based on literature data, with distributions chosen to ensure representative coverage. For instance, a truncated normal distribution was utilized for permeability to predominantly reflect lower values observed in the literature. The ranges for porosity and permeability remained consistent across all cases, while the range for initial reservoir pressure varied with changes in PVT templates to ensure the initial value exceeded the bottomhole flowing pressure of the producer well, set above the MMP. The maximum oil rate was capped at 5000 STB/D, the gas injection rate at 10,000 MSCF/D, and the bottomhole injection pressure limit at 6000 PSI to encompass a broad spectrum of scenarios.

The input ranges for porosity, permeability, and initial pressure were compared to the ranges observed in field cases gathered from literature sources as shown in Figure 13. Analysis of the scatter plot reveals that porosity exhibits a linear distribution encompassing the full range of field data. Permeability distribution predominantly clusters within the 0–200 mD range, with fewer cases observed beyond this range. Conversely, the distribution of initial pressure covers the entire field data range, with a notable concentration of cases at higher values exceeding 2500 PSI. This concentration aligns with expectations, as the input values were deliberately selected to surpass the Minimum Miscibility Pressure (MMP).

The post-simulation analysis revealed that the simulated data spans the spectrum of recovery factors and hydrocarbon pore volume injected observed in field operations. However, the P50 recovery factor derived from simulation data appears more optimistic compared to field data. This disparity can be attributed to the fact that injection in simulation scenarios commenced from day 1, facilitating pressure maintenance and resulting in higher recovery rates. In contrast, much of the recovery data reported in the literature pertains to secondary or tertiary recovery, indicating incremental gains, which consequently exhibit lower values compared to simulations, although simulation data spans the entire range, the P50 value is notably higher in simulations, as illustrated in Figure 14.



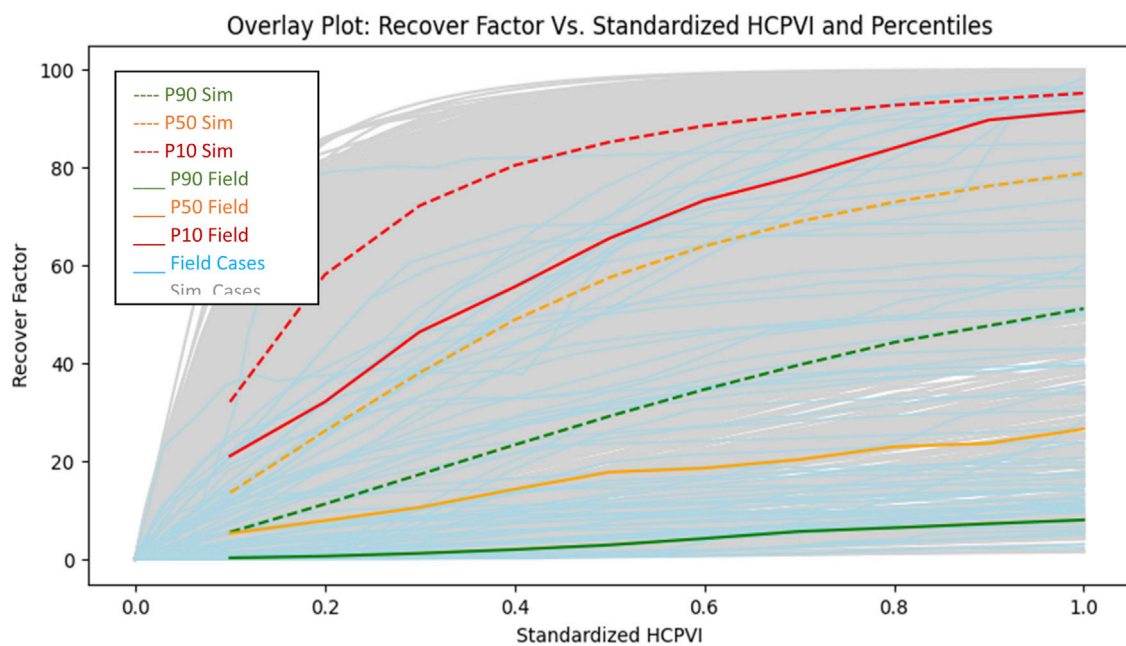


FIGURE 14  
Recovery factor versus standardized hydrocarbon pore-volume injected simulation results compared with field data.

## 6 Proxy model development

Proxy models are constructed by leveraging established models with reliable outcomes, wherein parameters deemed influential are selected for a fitting process. This process estimates results for additional cases if input values fall within the parameter range used to construct the proxy model (Bahrami et al., 2022). Artificial Neural Networks (ANNs) draw inspiration from the functioning of biological neurons in the human brain. The network comprises an input layer representing input parameters, an output layer indicating the target parameter to be predicted, and multiple hidden layers in between. Neurons within each layer are computed based on preceding layer neurons, weights, and a bias factor (Mohaghegh, 2000). In our study, ANN was employed to develop a proxy model for predicting oil flow rate ( $Q_o$ ), gas rate ( $Q_g$ ), and  $CO_2$  production. Optimal fit and accurate predictions were achieved through testing various configurations of neurons and layers. Input parameters were categorized into reservoir parameters, such as initial reservoir pressure, porosity, permeability, relative permeability templates, and PVT/fluid composition templates, and operational parameters, including gas injection rate, bottomhole injection pressure, and bottomhole flowing pressure. The ranges of input data are detailed in Table 3:

To ensure uniformity in input data scales and prioritize parameters equally in the model's initial impact, data standardization was executed. This process was guided by the mathematical expression outlined by Equation 6 (Muther et al., 2021):

$$x_{standard} = \frac{x - Mean}{Standard\ Deviation} \quad (6)$$

Where  $x$  is the value of each parameter in the input or output data.

To assess the impact of each input parameter on the target output parameter, we employed the Random Forest Regressor method. This approach involves partitioning the data into subsets and evaluating the variance reduction for each attribute at every tree level (Ho, 1995, p. 1). This technique is utilized to determine the importance of input parameters, irrespective of whether they contribute to an increase or decrease in the output (Belyadi and Haghighat, 2021).

It's observed in Figure 15 that time holds the most significant influence on production, as anticipated, followed by porosity. Conversely, initial pressure exhibits the least impact on production, as anticipated, given that once  $CO_2$  injection commences, it can surpass initial pressure values and exert a greater influence.

The dataset is divided into an 80% portion for training the model and adjusting weights, while the remaining 20% is further divided into two equal parts: 50% serves as a testing dataset for evaluating prediction accuracy, and the remaining 50% acts as a validation set to assess model performance. Additionally, we employ 10-fold cross-validation by default during the splitting process to minimize the risk of overfitting and ensure robust model evaluation. As previously discussed, the model's architecture comprises layers and nodes, with each node's calculation based on preceding layer nodes, their weights, and a bias factor. An activation function is employed to constrain each node's output value within the range of 0–1, aiding in capturing nonlinear relationships between nodes. The Rectified Linear Unit (ReLU) activation function was utilized in this study. Optimization algorithms are used to improve the accuracy and robustness of searching for the optimum weight factors for achieving the minimum objective function by adjusting the learning rate. The algorithm we used is 'Adam', which is suitable for large dataset problems; it is based on adjusting lower-order moments (Kingma and Ba, 2017).

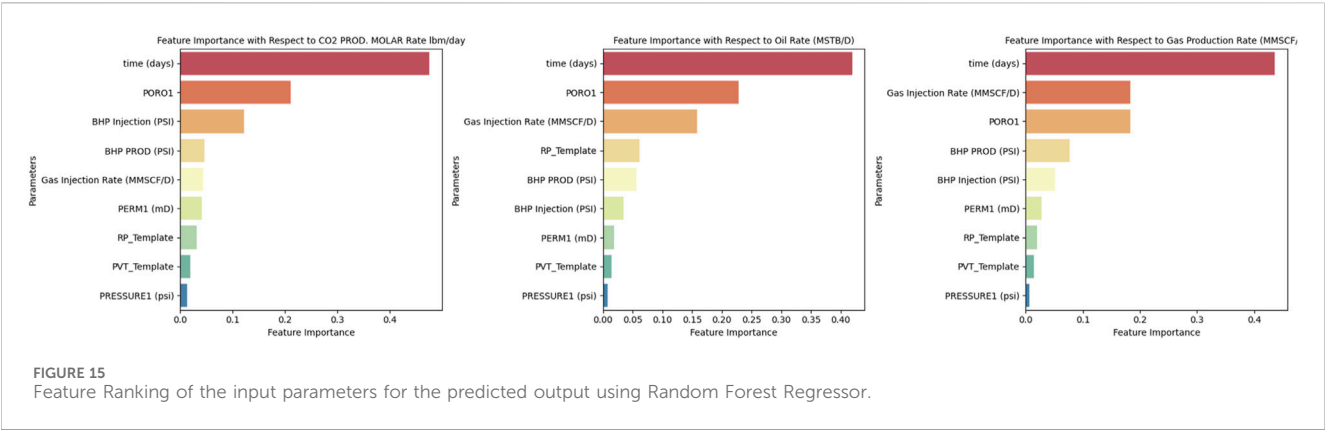


TABLE 3 Proxy model input data range.

Parameter	Range
Initial Reservoir Pressure (Psi)	1,500–5,000
Porosity (Fraction)	0.05–0.385
Permeability (mD)	2–980
Relative Permeability (RP) Template	1–9
Fluid Composition (PVT) Templates	1–8
Gas Injection Rate (MMSCF/D)	0–10,000
Bottom Hole Injection Pressure (Psi)	1,495–6,000
Bottom Hole Flowing Pressure (Psi)	1,470–4,764

The neural network model aims to determine optimal weights that minimize the objective function. In the case of a regression neural network, this objective function can be one of several regression evaluation metrics, such as mean absolute error (MAE), mean squared error (MSE), and root mean squared error (RMSE). In our model generation process, we utilized MAE as the objective function, while employing other metrics for model evaluation. MAE computes the average absolute difference between actual and predicted values, expressed by the formula (Belyadi and Haghighat, 2021) where  $n$  represents the number of sample points,  $y_i$  denotes the actual output, and  $\hat{y}_i$  represents the predicted output from the model as shown in Equation 7:

$$\frac{1}{n} \sum_{i=1}^n |y_i - \hat{y}_i| \tag{7}$$

The evaluation of the proxy model involved several stages. The initial stage involved plotting the loss function against the trained epoch numbers. Ideally, as the ANN model undergoes training, the loss function should diminish with increasing epoch numbers. A well-trained model is expected to exhibit decreasing loss values for both the training and testing datasets, as depicted in Figure 16 for the three outputs of the proxy model.

The second evaluation stage involves creating a cross-plot to compare the actual simulation results with the predictions from the trained neural network (NN) model, both presented in their standardized form. This plot demonstrates a strong correlation,

as illustrated in Figure 17. Although some data points may appear scattered, the overall results are consistent and satisfactory.

Another evaluation stage was establishing the performance metrics, which quantify the variance between the predicted outcomes from the proxy model and the actual results from the simulation. These metrics, shown in Table 4, reveal positive outcomes, demonstrating an acceptable level of accuracy across all three outputs.

The final evaluation checkpoint involves plotting individual cases. It was observed that the majority of cases exhibit a precise alignment. One interesting observation demonstrating the robustness of the training and testing process to ensure the generalization capability of the trained proxy models without memorization or overtraining is their insensitivity to noise. We deliberately included the results of some cases, as illustrated in Figure 18, where oscillations in the simulation results are observed due to convergence during numerical simulation. However, the trained proxy model did not incorporate these oscillations and noise but instead accurately captured the simulation’s underlying physical trend.

## 7 Screening and designing applications

The utilization of the trained ANN proxy model depends on the phase of the CO<sub>2</sub> project under consideration. In the initial design stage, where data availability is limited, primarily sourced from analog or neighboring fields, numerous uncertainties arise. During this phase, the aim of employing the proxy model is to swiftly assess the spectrum of outcomes for various scenarios and their economic feasibility.

Imagine a fresh field where we’re aiming to introduce CO<sub>2</sub> EOR. The uncertainties we confront are having two different possible fluid composition templates; template 1 or 8, three different relative permeability templates; template 1, 2 or 3, three porosity values 0.06, 0.12 or 0.16, and three permeability values 8 mD, 16 mD or 32 mD. Employing the ANN Proxy model allows us to generate diverse scenarios that tackle these uncertainties. Consequently, we can obtain approximations of the highest, median, and lowest production profiles, illustrated in Figure 19. These profiles serve as inputs for conducting techno-economic analyses. Furthermore, the proxy model can be used to predict the amount of produced CO<sub>2</sub> in moles. By combining this with the injected CO<sub>2</sub> moles, the CO<sub>2</sub> retention factor can be estimated using Equation 1.

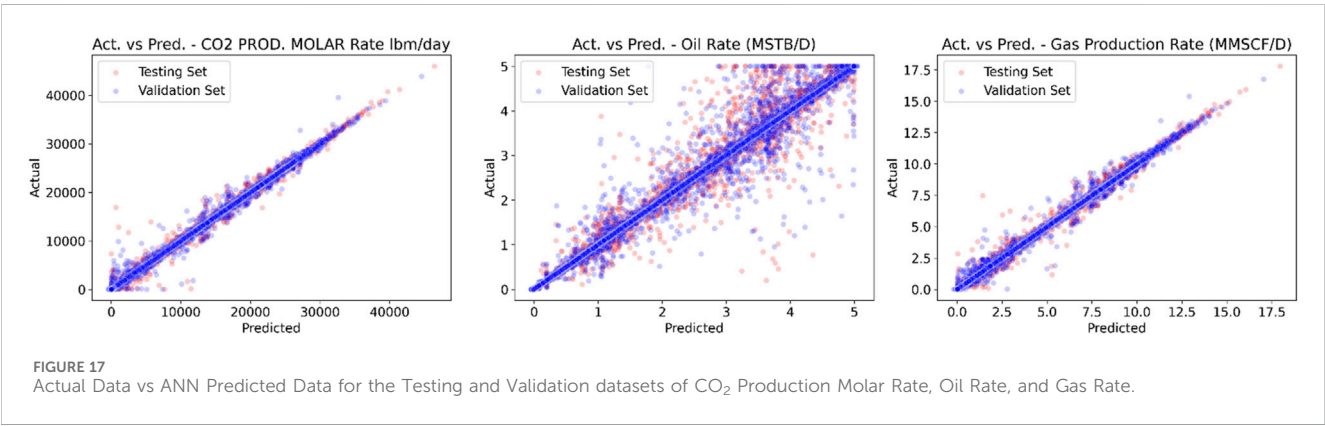
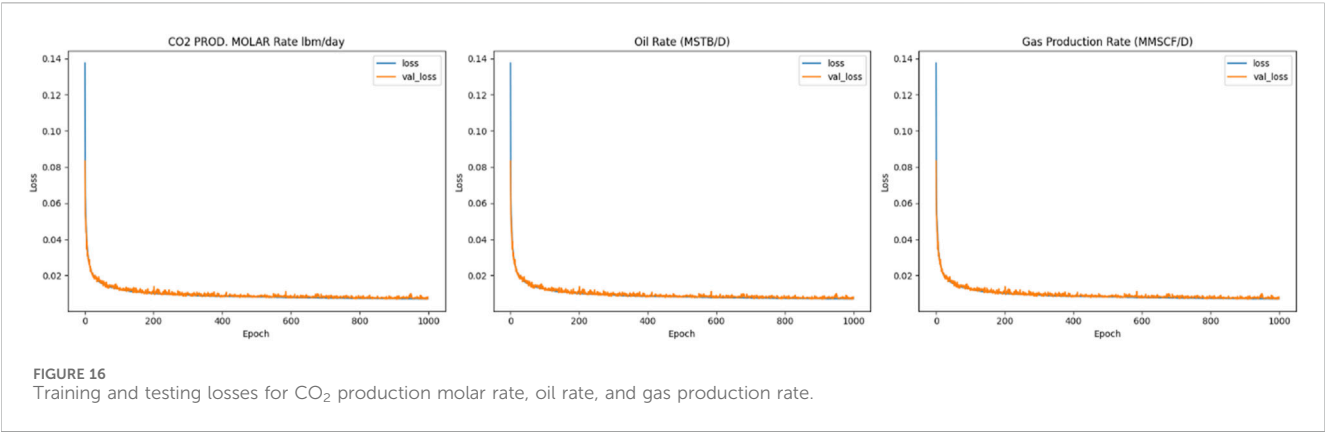


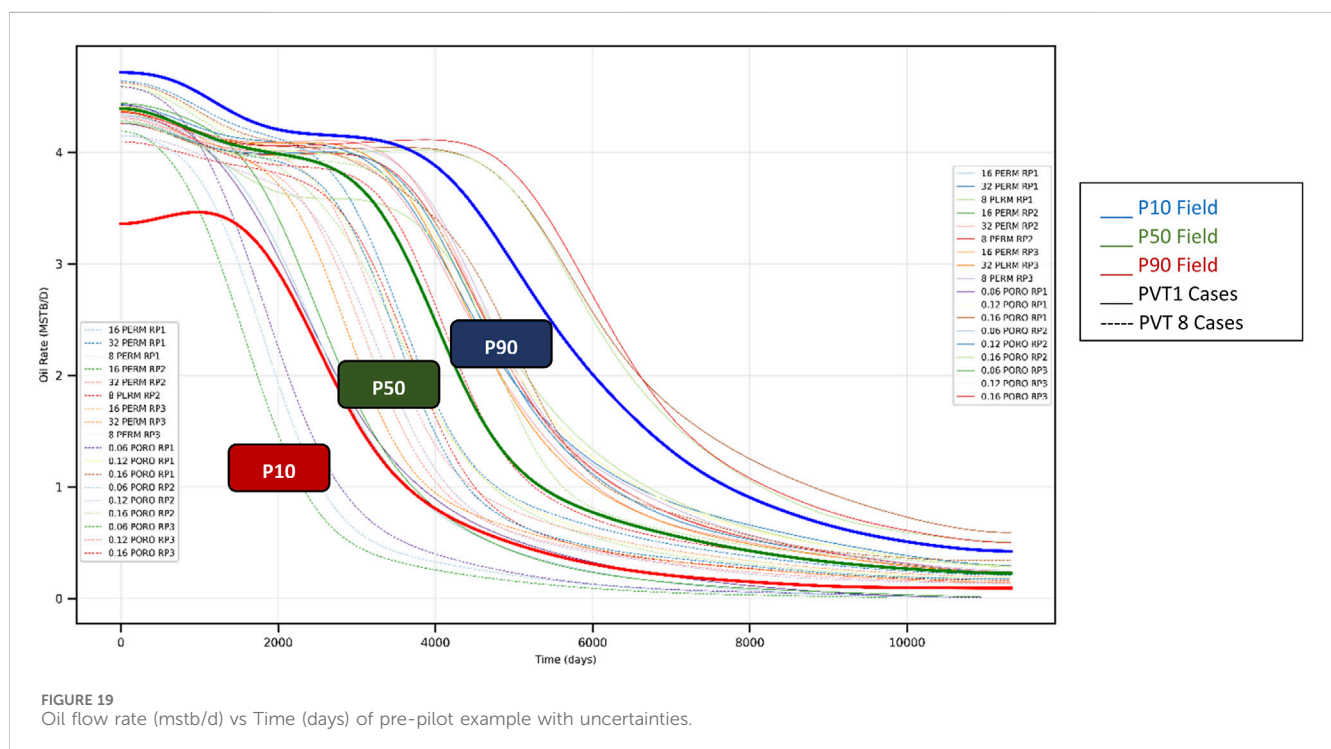
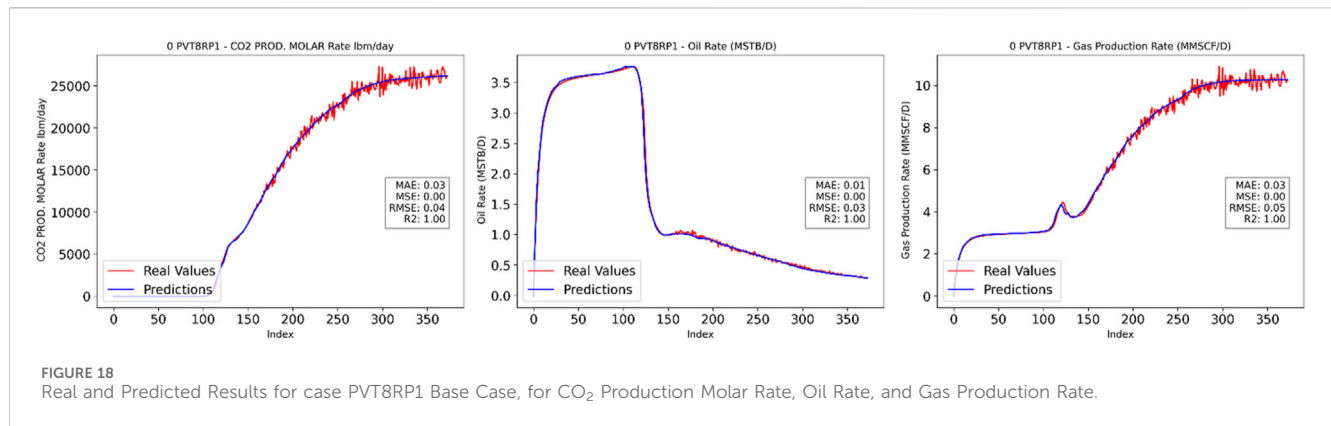
TABLE 4 Performance metrics between actual and proxy model outputs.

Performance metrics	Formulae	Validation			Training			Testing		
		CO <sub>2</sub>	Oil	Gas	CO <sub>2</sub>	Oil	Gas	CO <sub>2</sub>	Oil	Gas
Mean Absolute Error (MAE)	$\frac{1}{n} \sum_{i=1}^n  y_i - \hat{y}_i $	0.00553	0.012384	0.0068	0.0053	0.0108	0.0058	0.0055	0.011	0.0061
Mean Squared Error (MSE)	$\frac{1}{n} \sum_{i=1}^n (y_i - \hat{y}_i)^2$	0.00028	0.002746	0.0004	0.0002	0.002	0.0003	0.0003	0.0026	0.0004
Root Mean Squared Error (RMSE)	$\sqrt{\frac{1}{n} \sum_{i=1}^n (y_i - \hat{y}_i)^2}$	0.01695	0.052411	0.0203	0.015	0.048	0.017	0.017	0.051	0.02
Correlation of Coefficient (R2)	$R^2 = 1 - \frac{\sum (y_i - \hat{y}_i)^2}{\sum (y_i - \bar{y})^2}$	0.99971	0.997254	0.9995	0.9997	0.997	0.999	0.9996	0.997	0.999
Mean Absolute Percentage Error (MAPE)	$\frac{1}{n} \sum_{i=1}^n \frac{ y_i - \hat{y}_i }{y_i} \times 100$	3.609%	6.722%	2.76%	3.03%	10.31%	3.068%	2.414%	9.46%	2.427%

## 8 Post-pilot application

The ANN Proxy model was utilized to create type curves representing the dimensionless oil rate (Qd) and its first derivative against dimensionless time (tD). This involved employing 8 fluid composition templates and 9 relative permeability templates while adjusting porosity, permeability, and initial pressure. As we transition into the post-pilot stage, where data

collection begins and production profiles emerge, these dimensionless type curves serve to refine the remaining missed reservoir data. For instance, suppose the pilot well operation yields a production profile akin to the dotted plot depicted in Figure 20. By aligning this profile with the type curves generated by the proxy model, we can infer its resemblance to a scenario characterized by the fluid composition of template 1, relative permeability curves of template 2, a permeability of 16 mD, porosity of 0.12, and an initial



pressure of 3000 PSI Figure 21. Importantly, this method extends beyond the values illustrated in the type curves; interpolated values can also be derived using the same proxy model, thereby enhancing its applicability across a broader spectrum of scenarios.

## 9 Summary and conclusion

In summary, various reservoir characteristics significantly influence the production behavior of both CO<sub>2</sub>-EOR projects and CO<sub>2</sub> storage endeavors. Advancements in machine learning can support both design and implementation phases. Key findings from this study include:

- Sensitivity analysis indicates that while some properties, such as initial reservoir pressure, have a slightly lesser impact on production profiles, dimensionless type curves provide a

distinctive response that characterizes reservoir behavior effectively.

- The proposed ANN-based proxy model (PM) offers a computationally efficient alternative to traditional simulation methods for candidate reservoir screening. Each traditional simulation case took an average of 20–45 min, whereas the PM generated results in seconds.
- The accuracy of the PM was validated through performance metrics, with a correlation coefficient of approximately 0.99 and a mean absolute error of 0.012 in oil rate predictions compared to actual values. Overfitting was carefully managed by ensuring that the model captured physical trends without mirroring simulation noise. However, further testing on actual field data is recommended to evaluate the PM's reliability.
- Utilizing dimensionless type curves allowed for additional applications during the post-production phase. This

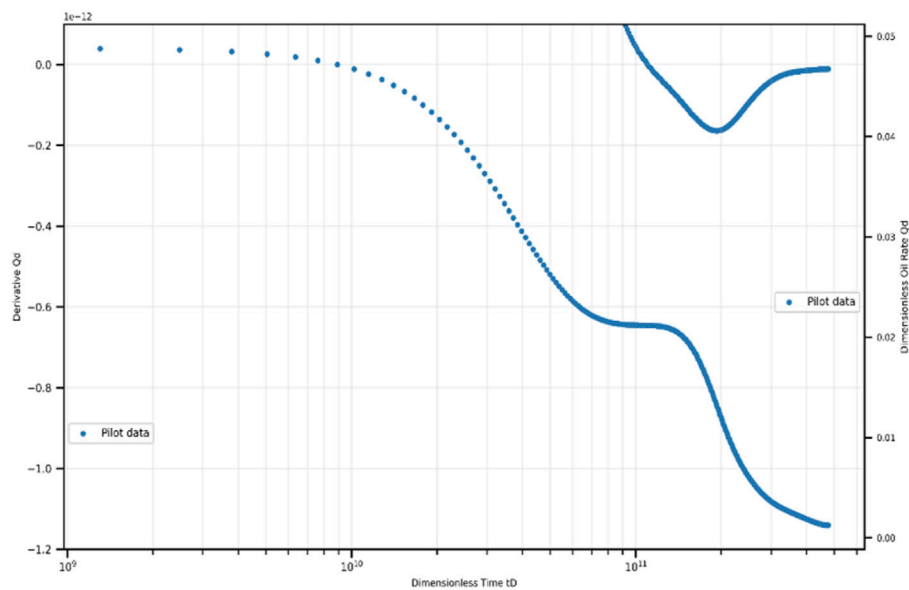


FIGURE 20  
Dimensionless Oil Rate and its First Derivative vs Dimensionless Time for Post-Production Application Pilot Data Example.

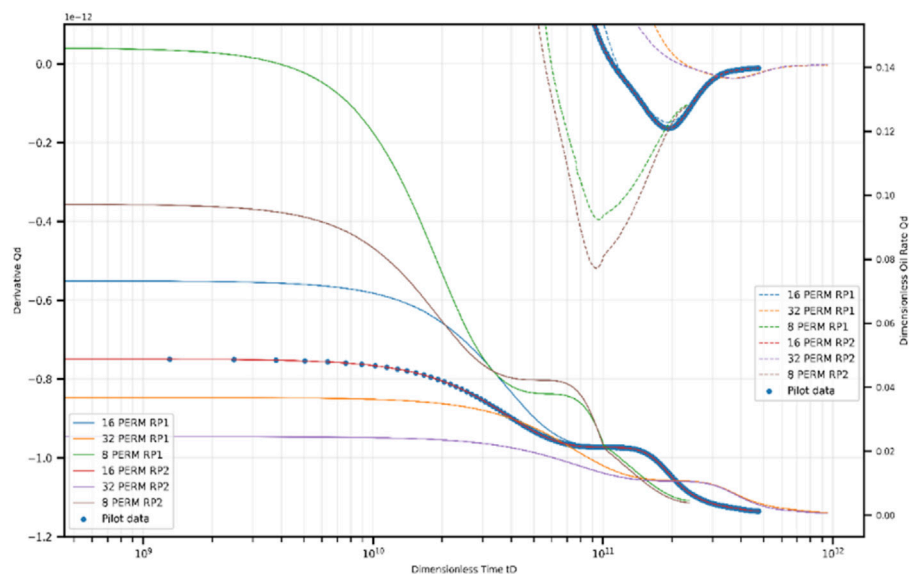


FIGURE 21  
Dimensionless Oil Rate and its First Derivative vs Dimensionless Time for Post-Production Application Example After Matching.

approach demonstrated effectiveness for oil rate predictions and could potentially be extended to other output metrics, such as gas rate and CO<sub>2</sub> molar production rate.

- The use of first derivatives of dimensionless oil rates in this study allows for more precise diagnostics of reservoir properties, including identifying trends such as pre-decline stability, breakthrough behavior, and post-decline production stabilization.

## 10 Limitations

The limitations identified in this study highlight opportunities for further research and development:

- The proxy model is valid and applicable only to reservoirs with properties that fall within the range of the training dataset.
- The fluid composition and relative permeability templates used in this study are fixed values, although they cover



most of the parameter ranges found in existing CO<sub>2</sub>-EOR projects.

- While this paper presents the methodology and its application, the results were not validated using actual field data.
- The proxy model was developed based on continuous CO<sub>2</sub> injection scenarios. Alternative methods, such as water-alternating gas (WAG) injection, are not covered by the current model. However, the study can be extended to include these methods.
- Operational changes, such as variations in the bottomhole flowing pressure, were not considered; this parameter was kept constant in all simulation cases.
- Well geometry, tubing, and casing configurations were assumed to be constant across all cases. Future studies could explore sensitivities to these parameters.

## Data availability statement

The raw data supporting the conclusions of this article will be made available by the authors, without undue reservation.

## Author contributions

RE: Data curation, Formal Analysis, Investigation, Validation, Visualization, Writing—original draft. AD: Conceptualization, Investigation, Methodology, Project administration, Supervision, Validation, Writing—review and editing.

## Funding

The author(s) declare financial support was received for the research, authorship, and/or publication of this article. Gratefully

acknowledges the financial support for this research for Raghda Emera provided by the Fulbright U.S. Student Program, sponsored by the U.S. Department of State and the binational Fulbright Commission in Egypt.

## Acknowledgments

Its contents are solely the responsibility of the authors and do not necessarily represent the official views of the Fulbright Program, the Government of the United States, or the binational Fulbright Commission in Egypt.

## Conflict of interest

The authors declare that the research was conducted in the absence of any commercial or financial relationships that could be construed as a potential conflict of interest.

## Publisher's note

All claims expressed in this article are solely those of the authors and do not necessarily represent those of their affiliated organizations, or those of the publisher, the editors and the reviewers. Any product that may be evaluated in this article, or claim that may be made by its manufacturer, is not guaranteed or endorsed by the publisher.

## Supplementary material

The Supplementary Material for this article can be found online at: <https://www.frontiersin.org/articles/10.3389/fenrg.2025.1478473/full#supplementary-material>

## References

- Ahmadi, M. A., Zendejboudi, S., and James, L. A. (2018). Developing a robust proxy model of CO<sub>2</sub> injection: coupling Box–Behnken design and a connectionist method. *Fuel* 215, 904–914. doi:10.1016/j.fuel.2017.11.030
- Aladasani, A., and Bai, B. (2010). “Recent developments and updated screening criteria of enhanced oil recovery techniques,” in *Presented at the international oil and gas conference and exhibition in China: Opportunities and Challenges in a Volatile Environment*. Richardson, TX: Society of Petroleum Engineers 1, 747–770. doi:10.2118/130726-MS
- Arps, J. J. (1945). Analysis of decline curves. *Trans. AIME* 160, 228–247. doi:10.2118/945228-G
- Bahrami, P., Sahari Moghaddam, F., and James, L. A. (2022). A review of proxy modeling highlighting applications for reservoir engineering. *Energies* 15, 5247. doi:10.3390/en15145247
- Belyadi, H., and Haghighat, A. (2021). *Machine learning guide for oil and gas using Python: a step-by-step breakdown with data, algorithms, codes, and applications*. Oxford, United Kingdom: Gulf Professional Publishing.
- Bourdet, D., Ayoub, J. A., and Plard, Y. M. (1989). Use of pressure derivative in well-test interpretation. *SPE Form. Eval.* 4, 293–302. doi:10.2118/12777-PA
- Chen, B., and Pawar, R. J. (2019). Characterization of CO<sub>2</sub> storage and enhanced oil recovery in residual oil zones. *Energy* 183, 291–304. doi:10.1016/j.energy.2019.06.142
- Chen, Z., Huan, G., and Ma, Y. (2006). *Computational methods for multiphase flows in porous media*. Philadelphia, PA: Society for Industrial and Applied Mathematics. doi:10.1137/1.9780898718942
- Claridge, E. L. (1972). Prediction of recovery in unstable miscible flooding. *Soc. Petroleum Eng. J.* 12, 143–155. doi:10.2118/2930-PA
- Dean, E., French, J., Pitts, M., and Wyatt, K. (2018). “Practical EOR agents - there is more to EOR than CO<sub>2</sub>,” in *Presented at the SPE EOR conference at oil and gas west asia*. Richardson, TX: Society of Petroleum Engineers. doi:10.2118/190424-MS
- Doublet, L. E., and Blasingame, T. A. (1995). Decline curve analysis using type curves: water influx/waterflood cases. *paper SPE 30774*, 22–25.
- Fetkovich, M. J. (1973). “Decline curve analysis using type curves,” in *Presented at the fall meeting of the society of Petroleum engineers of AIME*. Richardson, TX: Society of Petroleum Engineers. doi:10.2118/4629-MS
- Fetkovich, M. J., and Vienot, M. E. (1984). Rate normalization of buildup pressure by using afterflow data. *J. Petroleum Technol.* 36, 2211–2224. doi:10.2118/12179-PA
- Gao, P., Towler, B., and Pan, G. (2010). “Strategies for evaluation of the CO<sub>2</sub> miscible flooding process,” in *Proceedings of the Abu Dhabi international petroleum exhibition and conference* (Richardson, TX: Society of Petroleum Engineers), SPE-138786.
- Ghg, I. (2009). CO<sub>2</sub> storage in depleted oilfields: global application criteria for carbon dioxide enhanced oil recovery, 12. Cheltenham Glos, UK: Prepared by Advanced Resources International and Melzer Consulting.
- Ho, T. K. (1995). Random decision forests. *Proc. 3rd Int. Conf. Document Analysis Recognit. Present. A. T. Proc. 3rd Int. Conf. Document Analysis Recognit.* 1, 278–282. doi:10.1109/ICDAR.1995.598994
- Holm, L. W., and Josendal, V. A. (1974). Mechanisms of oil displacement by carbon dioxide. *J. Petroleum Technol.* 26, 1427–1438. doi:10.2118/4736-PA
- Holm, L. W., and Josendal, V. A. (1982). Effect of oil composition on miscible-type displacement by carbon dioxide. *Soc. Petroleum Eng. J.* 22, 87–98. doi:10.2118/8814-PA

- Iskandarov, J. S., Fanourgakis, G., Ahmed, S., Alameri, W., E. Froudakis, G., and N. Karanikolos, G. (2022). Data-driven prediction of *in situ* CO<sub>2</sub> foam strength for enhanced oil recovery and carbon sequestration. *RSC Adv.* 12, 35703–35711. doi:10.1039/D2RA05841C
- Klins, M. A. (1984). *Carbon dioxide flooding: basic mechanisms and project design*. Boston, MA: International Human Resources Development Corporation.
- Kingma, D. P., and Ba, J. (2014). *Adam: A method for stochastic optimization*. Ithaca, NY: Cornell University Library Available at: <https://arxiv.org/abs/1412.6980>.
- Kumar Pandey, R., Gandomkar, A., Vaferi, B., Kumar, A., and Torabi, F. (2023). Supervised deep learning-based paradigm to screen the enhanced oil recovery scenarios. *Sci. Rep.* 13, 4892. doi:10.1038/s41598-023-32187-2
- Le Quéré, C., Andrew, R. M., Canadell, J. G., Sitch, S., Korsbakken, J. I., Peters, G. P., et al. (2016). Global carbon budget 2016. *Earth Syst. Sci. Data* 8, 605–649. doi:10.5194/essd-8-605-2016
- McKay, M. D. (1992). "Latin hypercube sampling as a tool in uncertainty analysis of computer models," in *Proceedings of the 24th conference on winter simulation - WSC '92. Presented at the the 24th conference* (Arlington, Virginia, United States: ACM Press), 557–564. doi:10.1145/167293.167637
- Mohaghegh, S. (2000). Virtual-intelligence applications in Petroleum engineering: Part 1—artificial neural networks. *J. Petroleum Technol.* 52, 64–73. doi:10.2118/58046-JPT
- Muther, T., Syed, F. I., Dahaghi, A. K., and Neghabhan, S. (2021). "Subsurface physics inspired neural network to predict shale oil recovery under the influence of rock and fracture properties," in *2021 international conference on INnovations in intelligent SysTems and applications (INISTA). Presented at the 2021 international conference on INnovations in intelligent SysTems and applications (INISTA)* (Kocaeli, Turkey: IEEE), 1–6. doi:10.1109/INISTA52262.2021.9548580
- Novak Mavar, K., Gaurina-Medimurec, N., and Hrnčević, L. (2021). Significance of enhanced oil recovery in carbon dioxide emission reduction. *Sustainability* 13, 1800. doi:10.3390/su13041800
- NPC (2019). Meeting the dual challenge - report downloads. Available at: <https://dualchallenge.npc.org/> (Accessed 27 February, 2024).
- Olea, R. A. (2015). CO<sub>2</sub> retention values in enhanced oil recovery. *J. Petroleum Sci. Eng.* 129, 23–28. doi:10.1016/j.petrol.2015.03.012
- Orr, F. M., Jr. (2018). Carbon capture, utilization, and storage: an update. *SPE J.* 23, 2444–2455. doi:10.2118/194190-PA
- Taber, J. J., Martin, F. D., and Seright, R. S. (1997). EOR screening criteria revisited—Part 2: applications and impact of oil prices. *SPE Reserv. Eng.* 12, 199–206. doi:10.2118/39234-PA
- Tapia, J. F. D., Lee, J.-Y., Ooi, R. E. H., Foo, D. C. Y., and Tan, R. R. (2018). A review of optimization and decision-making models for the planning of CO<sub>2</sub> capture, utilization and storage (CCUS) systems. *Sustain. Prod. Consum.* 13, 1–15. doi:10.1016/j.spc.2017.10.001
- Yin, M. (2015). *CO<sub>2</sub> miscible flooding application and screening criteria (M.S.)*. Missouri University of Science and Technology. United States – Missouri.